SEMARAK ILMU PUBLISHING

Journal of Advanced Research in Fluid Mechanics and Thermal Sciences

Journal homepage:
https://semarakilmu.com.my/journals/index.php/fluid_mechanics_thermal_sciences/index
ISSN: 2289-7879

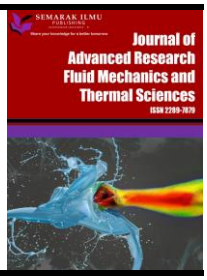

A Comparative Analysis of Aerodynamic Performance: Straight Fin and Curved Fin Rockets using Computational Fluid Dynamics (CFD)

Arief Dwi Nur Barokah[1], Ubaidillah[1,2,*], Bhre Wangsa Lenggana[3], Lasinta Ari Nendra Wibawa[4], Arjon Turnip[5], Endra Joelianto[6], Nguyen Le Hoa[7]

[1] Department of Mechanical Engineering, Faculty of Engineering, Universitas Sebelas Maret, Surakarta 57126, Indonesia
[2] Mechanical Engineering Department, Islamic University of Madinah, Madinah Al Munawwarah, 42351, Saudi Arabia
[3] Industrial Engineering Department, Universitas Jendral Soedirman, Indonesia
[4] National Research and Innovation Agency (BRIN), Central Jakarta, Indonesia
[5] Department of Electrical Engineering, Faculty of Mathematics and Natural Sciences, Universitas Padjadjaran, Indonesia
[6] Instrumentation and Control Research Group, Faculty of Industrial Technology, Institut Teknologi Bandung, Bandung, Indonesia
[7] University of Science and Technology, University of Danang, Danang City, Viet Nam

ARTICLE INFO

Article history:
Received 30 October 2023
Received in revised form 1 February 2024
Accepted 13 February 2024
Available online 15 March 2024

Keywords:
Aerodynamic; rocket; rocket fin; straight fin; curved fin

ABSTRACT

This investigation seeks to discern the aerodynamic differentials between rockets featuring straight fins and those with curved fins, focusing on the drag coefficient (cd), lift coefficient (cl), and moment coefficient (cm). Employing the computational fluid dynamics (CFD) methodology within ANSYS Fluent software, the research endeavors to provide comprehensive insights. The rockets under scrutiny share a common cylindrical body configuration, boasting a 70 mm diameter, a conical nose, and four symmetrically positioned fins along the lower body. The CFD analyses encompass subsonic Mach 0.6 and supersonic Mach 1.2 scenarios, with the angle of attack systematically varying from 0° to 25° at 5° intervals for each velocity setting. The outcomes of the simulations reveal notable trends: both cd and cl exhibit an upward trajectory, while cm experiences a decrement with escalating angles of attack and velocities. The culmination of Ansys CFD simulations for both rocket configurations unequivocally indicates superior flight performance for the straight fin rocket. This discernment is grounded in the observed amplification of drag and lift coefficients, coupled with the concomitant reduction in the moment coefficient, thus elucidating the nuanced aerodynamic distinctions between straight fin and curved fin rockets across varying flight conditions.

1. Introduction

Rockets represent a technology that has undergone extensive global development by scientists over an extended period. The conceptual origins of rockets can be traced back to 400 BC. Over the course of their evolution, rockets have served diverse purposes across different historical epochs, encompassing applications in warfare, commercial endeavors, testing procedures, and satellite deployment into Earth's orbit. Defining a rocket as a propelled projectile, its functioning hinges upon

* *Corresponding author.*
E-mail address: ubaidillah_ft@staff.uns.ac.id

https://doi.org/10.37934/arfmts.115.1.118

the thrust generated by the energy conversion engine within. This engine effectuates the conversion of chemical energy into the heat energy of burning fuel in the combustion chamber, ultimately producing thrust. The expulsion of combustion at the nozzle propels the rocket in the opposing direction to the thrust [1]. Within the realm of rocket development, the critical role of aerodynamic analysis in optimizing performance cannot be overstated. Of the various components influencing a rocket's aerodynamics, fins play a particularly significant role. These structures enhance flight stability and exhibit characteristics such as relatively modest dimensions, adaptable shapes tailored to mission requirements, and minimal drag. Additionally, they can generate lift in accordance with Bernoulli's Law, thereby mitigating the impact of turning momentum induced by wind gusts or internal factors [2].

Numerous scholars, including Dahalan *et al.,* [3], Zhang *et al.,* [4,5], Sethunathan *et al.,* [6], Eastman and Wenndt [7], have undertaken studies investigating the aerodynamic characteristics of straight and curved fin rockets, as well as the airflow dynamics over these fins. These investigations utilize diverse methodologies such as analytical techniques, wind tunnel experimentation, and Computational Fluid Dynamics (CFD) simulations. This present study focuses on elucidating the aerodynamic traits of distinct fin configurations, specifically curved and flat fins, at subsonic speeds of Mach 0.6 and supersonic Mach 1.2, with variations in the angle of attack ranging from 0 to 25 degrees. The study contributes to comprehending and identifying the aerodynamic efficiency of different fin designs, with performance curves aiding in discerning the superiority of each design under diverse flight conditions. Moreover, the examination delves into how alterations in the angle of attack impact the aerodynamic coefficients of both fin designs, shedding light on the optimal conditions for each design across a spectrum of flight scenarios.

In the realm of military applications, the prevalent deployment of curved fin rockets is pronounced, particularly in training and operational contexts. The selection of curved fin rockets is underpinned by their spatial efficiency, especially with regard to storage considerations. The curvature of these fins facilitates optimal storage within missile tubes, thereby conferring advantages such as diminished reloading necessities and the capacity to deploy a substantial quantity of rockets on the battlefield [3]. Notably, the curvature of these fins engenders significant aerodynamic forces and moments, a characteristic absent in planar or straight fin counterparts [7]. To discern and evaluate the aerodynamic performance disparity between straight and curved fin rockets, researchers have employed Computational Fluid Dynamics (CFD) simulations. CFD simulations involve the application of numerical methodologies within defined control volumes, integrating equations pertaining to mass, momentum, and energy balances to scrutinize fluid flow patterns [8].

Driven by considerations of expediency, cost-effectiveness, and data precision, numerous entities, spanning both the private sector and governmental domains, have transitioned from conventional testing methodologies to computational and numerical simulations utilizing Computational Fluid Dynamics (CFD). This paradigmatic shift represents the prevailing optimal approach for addressing challenges related to fluid flow or aerodynamic systems and for facilitating further scholarly inquiry. The term "aerodynamics," derived from the components "aero" (pertaining to air) and "dynamics" (indicative of motion), encapsulates the examination of fluid flow's influence on the motion of an object at a designated velocity [8]. The present simulation endeavors to determine the values of the Coefficient of Drag (Cd), Coefficient of Lift (Cl), and Coefficient of Moment (Cm) under subsonic speeds of 0.6 Mach and supersonic speeds of 1.2 Mach. Through the meticulous analysis of the Cd, Cl, and Cm values derived from this simulation, a nuanced comparison arises, elucidating the distinct aerodynamic performances inherent in rockets featuring straight fins and those adorned with curved fins (see Figure 1).

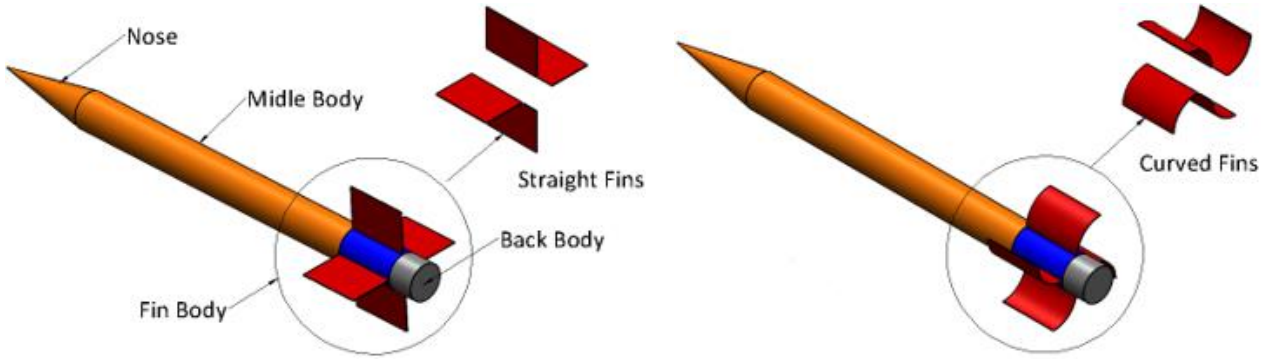

Fig. 1. (a) Straight fin rocket, (b) curved fin rocket

Rockets, encompassing spacecraft, missiles, or aerial vehicles, derive their propulsion from the combustion reactions of a propellant. This propulsive force emanates from the swift combustion or explosive reactions occurring within the rocket chamber, where one or more fuels are engaged. The propellant fuel, serving as the motive agent, undergoes a combustion process within the dedicated chamber [9]. This combustion yields exceedingly elevated pressure and temperature, subsequently expelled through the nozzle situated at the rocket's rear. Consequently, the expelled propellant propels the rocket forward [3]. Illustrated in Figure 2, a rocket comprises four primary components: the structural system, payload system, guidance system, and propulsion system.

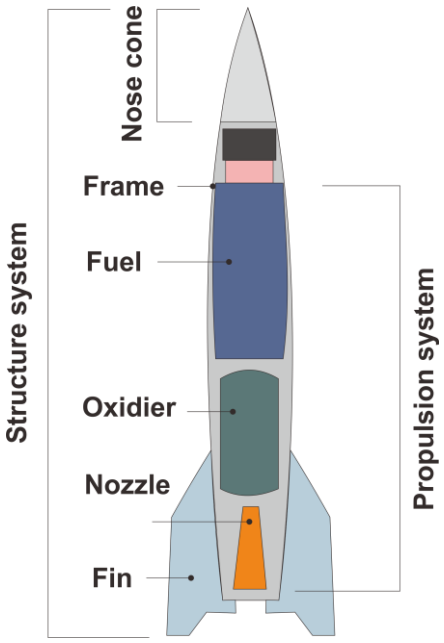

Fig. 2. Rocket parts

In the course of their flight, rockets undergo alterations in attitude, a phenomenon attributable to the interplay of internal and external forces and moments, as illustrated in Figure 3. Internally generated forces and moments contributing to these alterations emanate primarily from propulsion. Conversely, external factors contributing to attitude changes are instigated by gravitational forces and aerodynamic moments [1]. The genesis of aerodynamic moments lies in the rocket's traversal through the atmosphere, giving rise to a spectrum of forces, including pressure, frictional forces, lift, and drag. These forces are contingent upon the rocket's geometric configuration and the finishing techniques applied to its structural integrity.

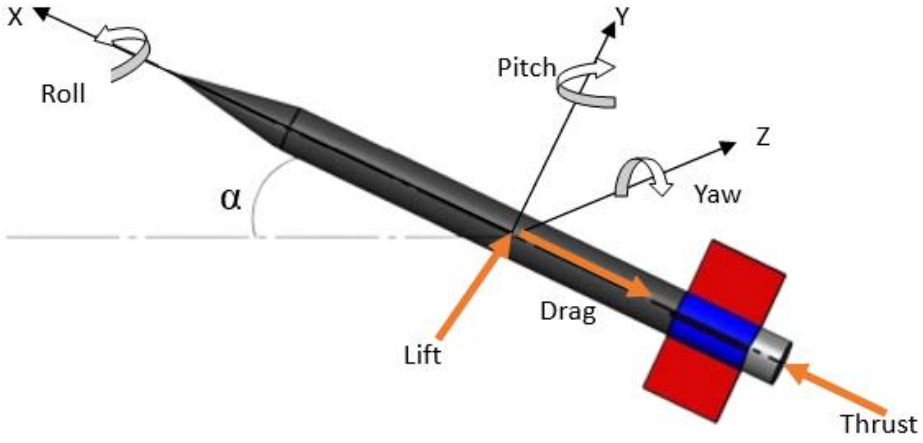

Fig. 3. Six (6) degrees of freedom rocket

The research article constitutes a significant contribution by employing computational fluid dynamics (CFD) methodology to discern the aerodynamic disparities between rockets featuring straight fins and those with curved fins. Through conducting CFD analyses across subsonic and supersonic scenarios while systematically varying the angle of attack, the research furnishes comprehensive insights into the aerodynamic behavior of these rockets. The outcomes underscore distinct trends, revealing that both drag and lift coefficients exhibit an upward trajectory, while the moment coefficient decreases with increasing angles of attack and velocities. This discernment contributes valuable knowledge to the understanding of nuanced aerodynamic distinctions between straight fin and curved fin rockets under varying flight conditions.

The Coefficient of Drag (Cd) constitutes a pivotal parameter governing the magnitude of drag force experienced by an object in motion. Defined as the force exerted on an object aligned parallel to the free stream, drag force arises due to pressure and shear stress on the object's surface as it traverses through a fluid, particularly in the context of gases such as air. Conversely, the Coefficient of Lift (Cl) denotes a dimensionless parameter intricately linked to the lift force acting on a body navigating through a fluid. The influence of the body's shape prominently shapes the Coefficient of Lift, a phenomenon particularly germane to rocket fins when immersed in a fluid medium, specifically air. In the context of rocketry, lift force manifests as the rocket maneuvers through the air. The airflow over the upper surface of the rocket fins surpasses the velocity of the air flowing along the lower surface. This disparate airflow engenders a discernible pressure gradient, resulting in lower pressure on the upper surface relative to the lower surface of the rocket fins. The consequential pressure imbalance induces an upward lift force, thereby contributing to the overall lift dynamics of the rocket—from its base to its apex [10].

$$Cd = \frac{2 \times Fd}{\rho \times v^2 \times A} \tag{1}$$

$$Fd = \frac{1}{2} \times \rho \times v^2 \times A \times Cd \tag{2}$$

$$Cl = \frac{2 \times Fl}{\rho \times v^2 \times A} \tag{3}$$

$$Fl = \frac{1}{2} \times \rho \times v^2 \times A \times Cl \tag{4}$$

The term "moment" in aeronautics denotes the rotational motion induced by forces that give rise to angular velocity relative to the aircraft's Center of Gravity (CoG). This rotational effect manifests along the X, Y, and Z axes, eliciting angular velocities denoted as P, Q, and R, which, in turn, produce corresponding aerodynamic moments designated as L, M, and N. The dynamic behavior of the aircraft encapsulates rolling (rotation about the X axis), pitching (rotation about the Y axis), and yawing (rotation about the Z axis) [11].

$$Cm = \frac{2 \times Fm}{\rho \times v^2 \times A} \tag{5}$$

$$Fm = \frac{1}{2} \times \rho \times v^2 \times A \times Cm \tag{6}$$

The numerical simulation undertaken in this investigation employed the Finite Volume Method (FVM) in conjunction with turbulence models to conduct flow simulations at Mach numbers of 0.6 and 1.2. The fluid flow under examination is presumed to be steady, viscous, and isothermal. Within the confines of isothermal conditions, the absence of temperature variations in the fluid flow is posited, thereby justifying the exclusion of the Energy Conservation Law from the analytical scope of this study [12]. Furthermore, the solution to this computational problem involves the application of equations governing turbulent kinetic energy and specific turbulent dissipation [13]. Consequently, the overarching governing equations for this research are articulated as follows

Steady Flow Equation

$$\frac{\partial v}{\partial t} = 0 \text{ atau V =V (x,y,z)} \tag{7}$$

Navier-Stokes Equation

$$x;\ \rho\left(u\frac{\partial u}{\partial x} + v\frac{\partial v}{\partial y} + w\frac{\partial w}{\partial z}\right) = -\frac{\partial p}{\partial x} + \mu\left(\frac{\partial^2 u}{\partial x^2} + \frac{\partial^2 u}{\partial y^2} + \frac{\partial^2 u}{\partial z^2}\right) \tag{8}$$

$$y;\ \rho\left(u\frac{\partial u}{\partial x} + v\frac{\partial v}{\partial y} + w\frac{\partial w}{\partial z}\right) = -\frac{\partial p}{\partial x} + \mu\left(\frac{\partial^2 u}{\partial x^2} + \frac{\partial^2 u}{\partial y^2} + \frac{\partial^2 u}{\partial z^2}\right) \tag{9}$$

$$z;\ \rho\left(u\frac{\partial u}{\partial x} + v\frac{\partial v}{\partial y} + w\frac{\partial w}{\partial z}\right) = -\frac{\partial p}{\partial x} + \mu\left(\frac{\partial^2 u}{\partial x^2} + \frac{\partial^2 u}{\partial y^2} + \frac{\partial^2 u}{\partial z^2}\right) \tag{10}$$

Turbulence Kinetic Energy Equation

$$\frac{\partial k}{\partial t} + U_j\frac{\partial k}{\partial x_j} = P_k - \beta * k\omega + \frac{\partial}{\partial x_j}\left[(v + \sigma_k v_T\frac{\partial k}{\partial x_j}\right] \tag{11}$$

Specific Dissipation Rate Equation

$$\frac{\partial \omega}{\partial t} + U_j\frac{\partial \omega}{\partial x_j} = \alpha S^2 - \beta\omega^2 + \frac{\partial}{\partial x_j}\left[(v+\sigma_\omega v_T\frac{\partial k}{\partial x_j}\right] + 2(1-F_1)\sigma_{\omega 2}\frac{1}{\omega}\cdot\frac{\partial k}{\partial x_i}\cdot\frac{\partial \omega}{\partial x_i} \tag{12}$$

2. Methodology

2.1 Geometric Modeling

The first step before conducting the CFD simulation to find the values of cd, cl, and cm is to create a 3D model of the curved fin rocket and the straight fin rocket. Figure 4 shows the difference in shape between the two rocket fins. To obtain comparative simulation results for the two rocket shapes, it is ensured that both rockets have the same surface area of 0.269 m². Table 1 and Table 2 show the general description of rocket fin and the fin parts.

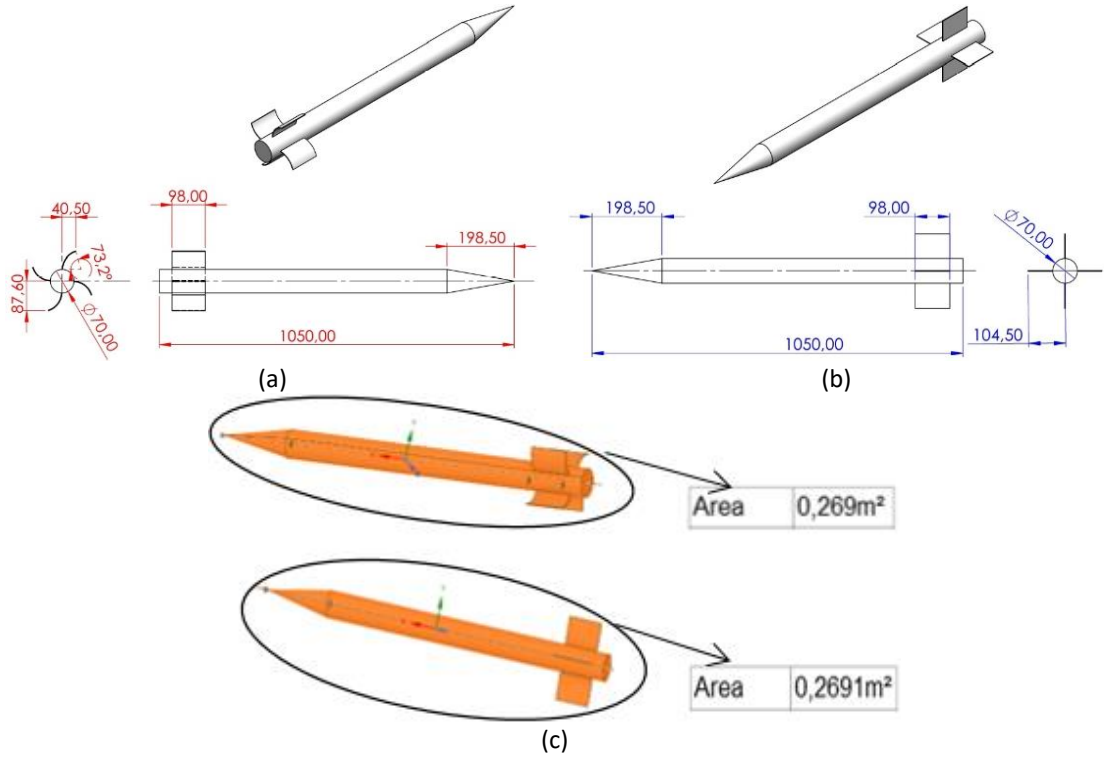

Fig. 4. (a) Geometry and dimensions of curved fin rockets (b) Geometry and dimensions of curved fin rockets (c) area of straight and curved fin rockets

Table 1
General description of curved fin and straight fin rockets

Rocket Model (body)	
Overall length, L	1050 mm
Body Diameter, D	70 mm
Nose Type, Length, l_N	Conical, 198,5 mm
Afterbody Length, l_A	851,5 mm
L/D ratio	15

Table 2
Fin parts description

Fin Model	
Fin Planform	Rectangular
Fin Configuration	Curved Fin and Flat Fin
Spanwise length of one fin	69,5 mm
Root chord	98 mm
Fin Thickness	2 mm
Fin Leading Edge Angle	0^0

2.2 Simulation

2.2.1 Enclosure

The 3D model is imported as an STP file to create the numerical fluid domain (enclosure). The dimensions and shape of the enclosure are adjusted according to the size of the test object, with a cylindrical shape as shown in Figure 5 having a diameter of 4 m and a length of 3.5 m in this experiment.

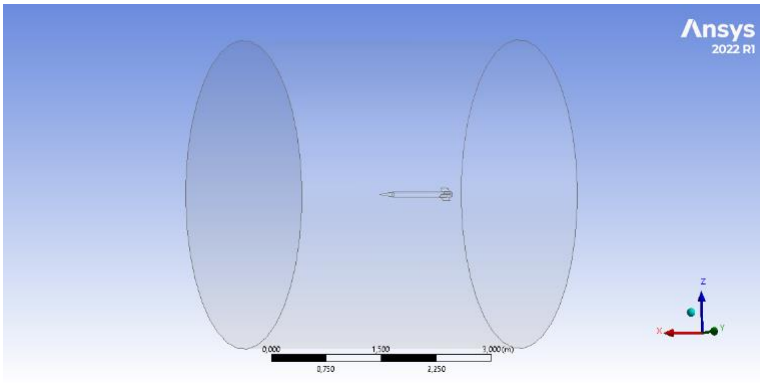

(a)

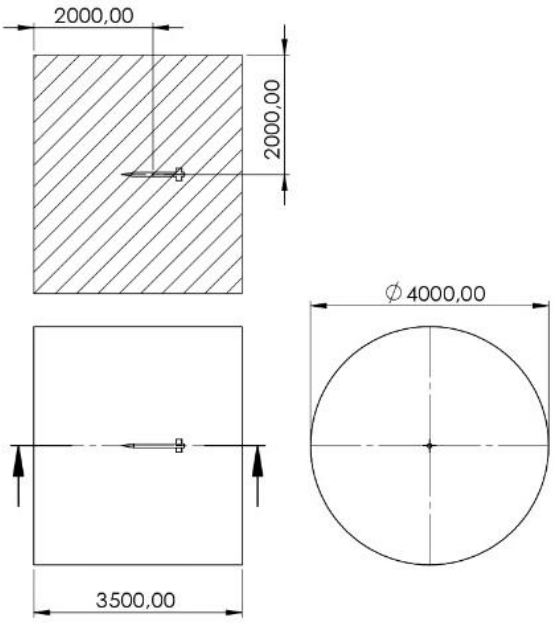

(b)

Fig. 5. (a) Cylinder Enclosure (b) Enclosure dimensions in mm

2.2.2 Meshing process

The meshing process (also known as discretization) in CFD simulation is the process of creating a discrete model of the geometric domain to be analyzed. This geometric domain is divided into small elements or cells called mesh or grid, allowing for numerical calculations using the underlying mathematical equations of CFD. Accurate analysis results can be achieved by using a large number of meshes, but an excessively dense mesh leads to longer solution times and data storage issues. Therefore, it is necessary to determine the optimal or stable mesh size for this research through a mesh independence test as shown in Figure 6.

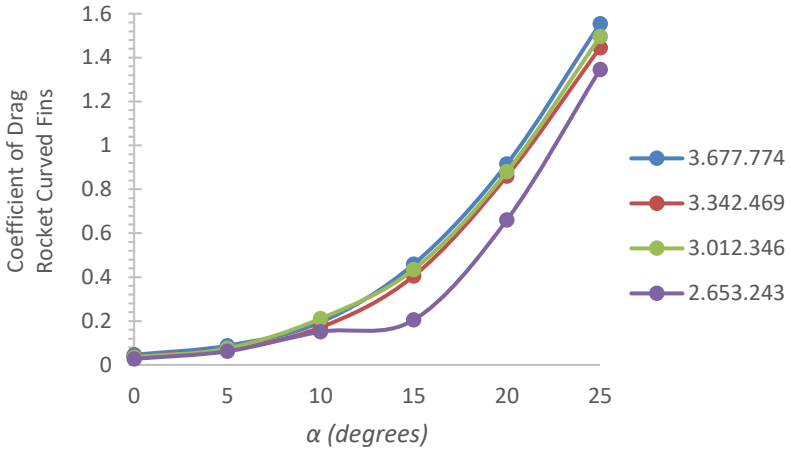

Fig. 6. Mesh Independent Test

The results of the mesh independence test conducted indicate that mesh sizes of 3,677,774, 3,342,469, and 3,012,346 show stable results. It can be concluded that simulation results with a number of meshes above (3,677,774-3,012,346) do not experience significant changes. Thus, it can be decided that the mesh size of 3,342,469 is an independent size for the simulation.

The mesh topology in this simulation uses tetrahedron elements (Figure 7). This is because it is easier to use and can handle complex geometries such as curved fins. The mesh quality after mesh treatment has an average skewness value of 0.22827. With an average skewness value close to 0 and an average orthogonal quality value close to 1, it proves that the mesh quality in this validation process is quite good.

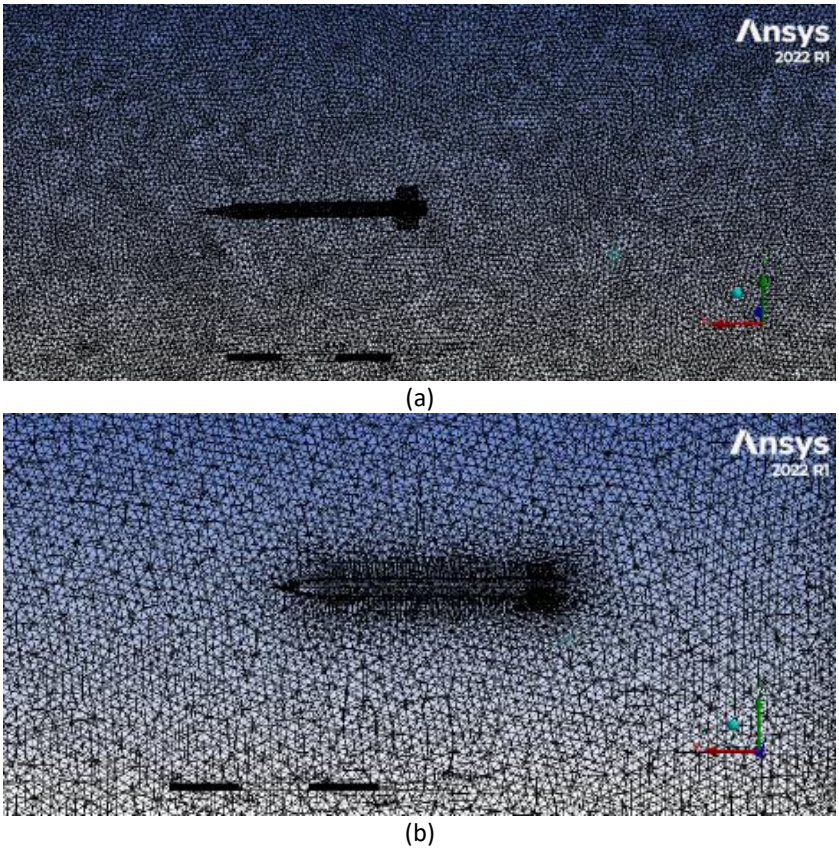

Fig. 7. (a) Tetrahedron Mesh on Rocket Straight Fins (b) Tetrahedron Mesh on Rocket Curved Fins

2.2.3 Boundary condition

The boundary condition (Figure 8) settings in this study referred to Dahalan's *et al.,* [3] research. The airflow was assumed to be steady flow and isothermal flow with a fluid density of 1.17 kg/m3 and a fluid viscosity of 1.7894x10-5 kg/ms. The boundary conditions at the inlet were velocity-inlet with velocities of 0.6 Mach and 1.2 Mach, and at the outlet, pressure-outlet (zero-gauge pressure condition) was used. The turbulence intensity at the inlet was 5%, which referred to low flying conditions and made the simulation results sensitive to stall conditions [14]. The outer side was considered an ideal wall with a shear stress of 0 to avoid errors in the simulation process due to limitations when altering the fluid domain, which was inherently unbounded but constrained by the dimensions of the enclosure [15]. Table 3 shows the reference values on the boundary conditions of straight fin and curved fin rockets.

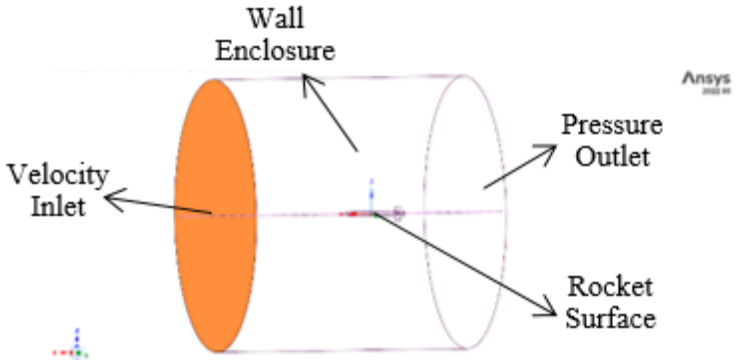

Fig. 8. Boundary Condition

Table 3
Reference values on the boundary conditions of straight fin and curved fin rockets

Parameters	Value	Unit
Density	1,17	kg/m^3
Cp (Specific Heat)	1006,43	J/(kg.K)
Thermal Conductivity	0,0242	W/(m.K)
Viscosity	1,7894 x 10-5	kg/(m.s)
Molecular Weight	28,966	kg/kmol
Velocity Inlet	204,174 and 408,348	m/s
Turbulent intensity	5	%
Turbulent Viscosity Ratio	10	
Pressure Outlet	0	Pa
Temperature	288.16	K
Length	1	m
Area	0,049875	m^2
Rocket Wall	No-slip condition	

The rocket surface was defined as a stationary wall subject to a no-slip condition. The application of the no-slip condition entailed adherence to the "log-law of the wall," leading to velocity distribution arising from shear stress on the boundary layer along the rocket surface [16]. The numerical solution method employed in this study was the k-omega SST turbulent model with a coupled scheme. The selection of the k-omega SST (Shear Stress Transport) turbulent model was based on its capacity to predict flow separation along the rocket and its consistency with experimental findings [17]. Moreover, the k-omega SST turbulent model was chosen due to its proficient performance in the vicinity of the wall region.

3. Results

3.1 Pressure Distribution

The results of the CFD simulation of the curved fin and straight fin rockets at speeds of 0.6 and 1.2 Mach and angles of attack (0-250) are displayed in the Figure 9. From these graphs, we can determine the values of Cd and Cl, which increase and Cm decreases with increasing angles of attack.

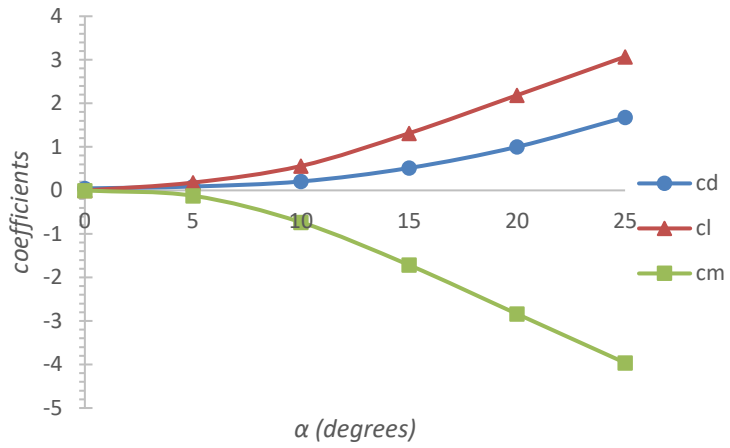

(a)

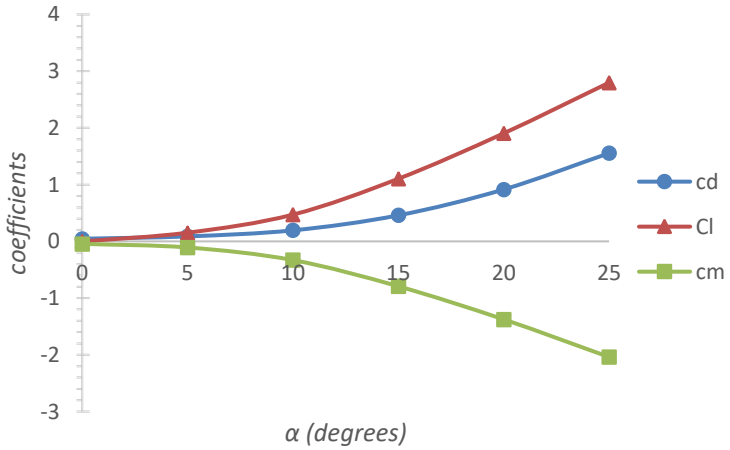

(b)

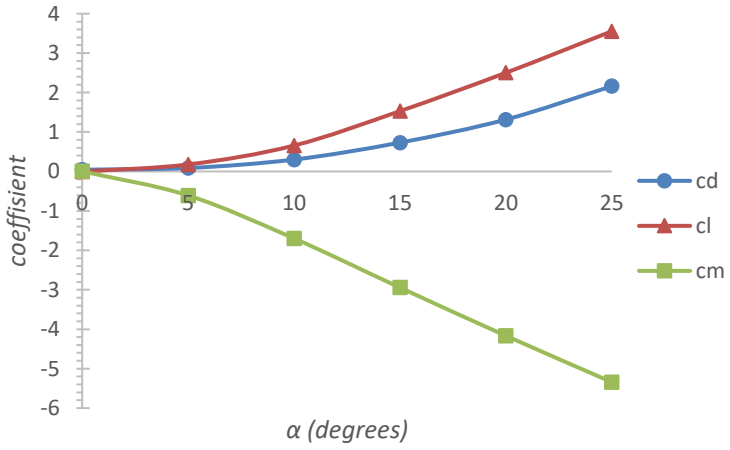

(c)

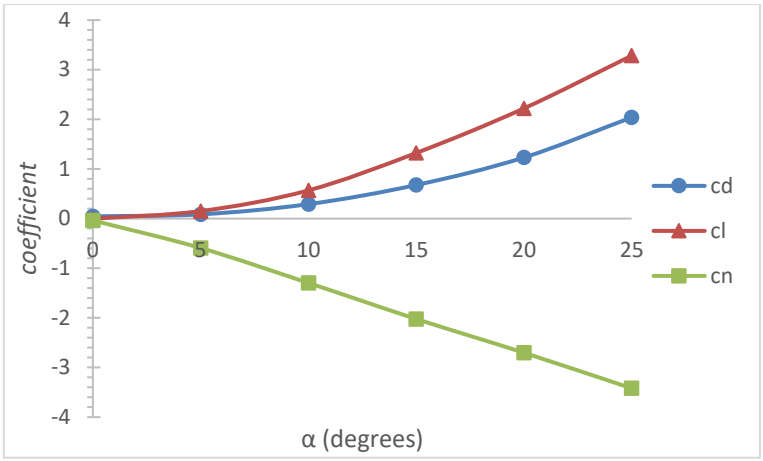

(d)

Fig. 9. (a) Mach 0.6 Straight Fin Rocket, (b) Mach 0.6 Curved Fin Rocket, (c) Mach 1.2 Straight Fin Rocket, (d) Mach 1.2 Curved Fin Rocket

The velocity and pressure contours from this simulation are also displayed in Figure 10, Figure 11, and Figure 12. In the velocity contour, separation points and separation flow on the rocket are observed. The separation point is visible as a red dot between the rocket's nose and body. The separation flow is indicated by the yellow colour on the top and rear of the rocket. At angles of attack (AoA) ranging from 0 to 100, clear flow separation on the rocket surface, especially on the top, is not yet apparent. However, at AoA values between 15 and 250, flow separation starts to become evident on the upper surface of the rocket, marked by the presence of yellow colour. The occurrence of separation flow at AoA values greater than 100 leads to a significant increase in drag force on the rocket.

In Figure 12, a notable distinction in pressure distribution between curved and straight fins is apparent. The dissimilarity in airflow patterns across the upper and lower surfaces of the fins leads to a pressure differential, resulting in the generation of lift force on the rocket. When the angle of attack (AoA) of a rocket is zero, the overall flow field exhibits symmetry concerning the upper and lower surfaces of the fin. Consequently, the pressure distribution on both surfaces of the fin is also symmetrical. In such instances, where the pressure difference between the upper and lower surfaces of the fin is negligible or nonexistent, the lift generated approaches zero. However, for fins positioned at a non-zero angle of attack, the flow field between their upper and lower surfaces becomes asymmetric. Consequently, fluid passing through the upper surface of the fin gains additional momentum due to the extended flow path compared to the lower surface. A straight-fin rocket typically displays a symmetrical pressure distribution between its upper and lower fin surfaces. Conversely, a curved-fin rocket exhibits an accumulation of pressure difference primarily on the inner portion of the fin. The pressure contour on the curved fin suggests that increasing the angle of attack may induce rotation or rolling.

From simulations conducted at velocities of 0.6 and 1.2 Mach, encompassing angle of attack values ranging from 0 to 250 degrees for both types of fins, it is observed that the drag coefficient (Cd) increases, with the straight-fin rocket registering the highest value. Examination of Figure 13 indicates that the Cd values between curved and straight fins are nearly equivalent, with a discernible discrepancy emerging at angle of attack values of 150-250. This divergence arises due to the straight fin's larger air contact area or greater pressure differential relative to the curved fin.

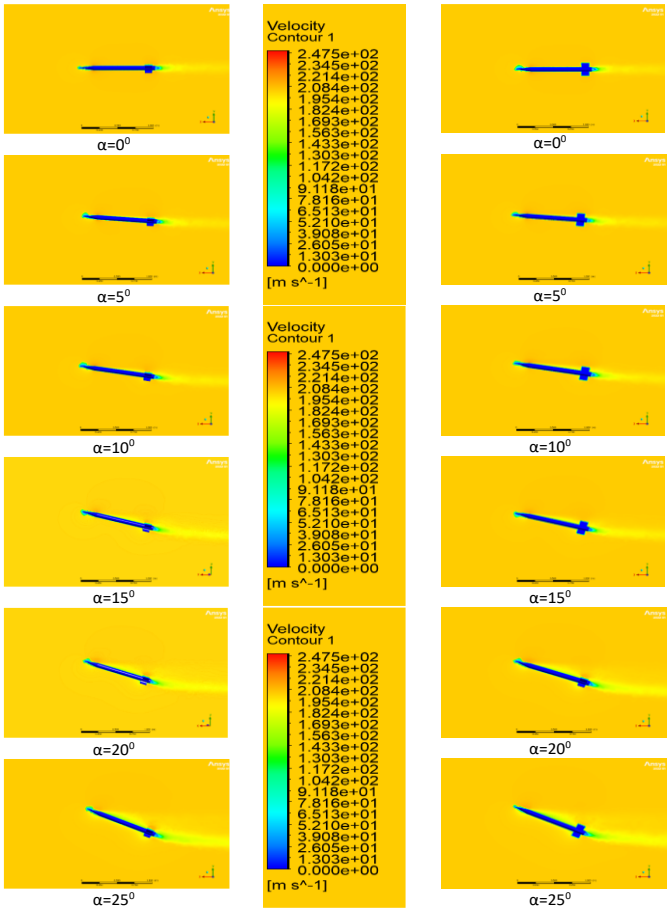

Fig. 10. (a) Mach 0.6 Curved Fin Velocity Contour Rocket (b) Mach 0.6 Straight Fin Velocity Contour Rocket

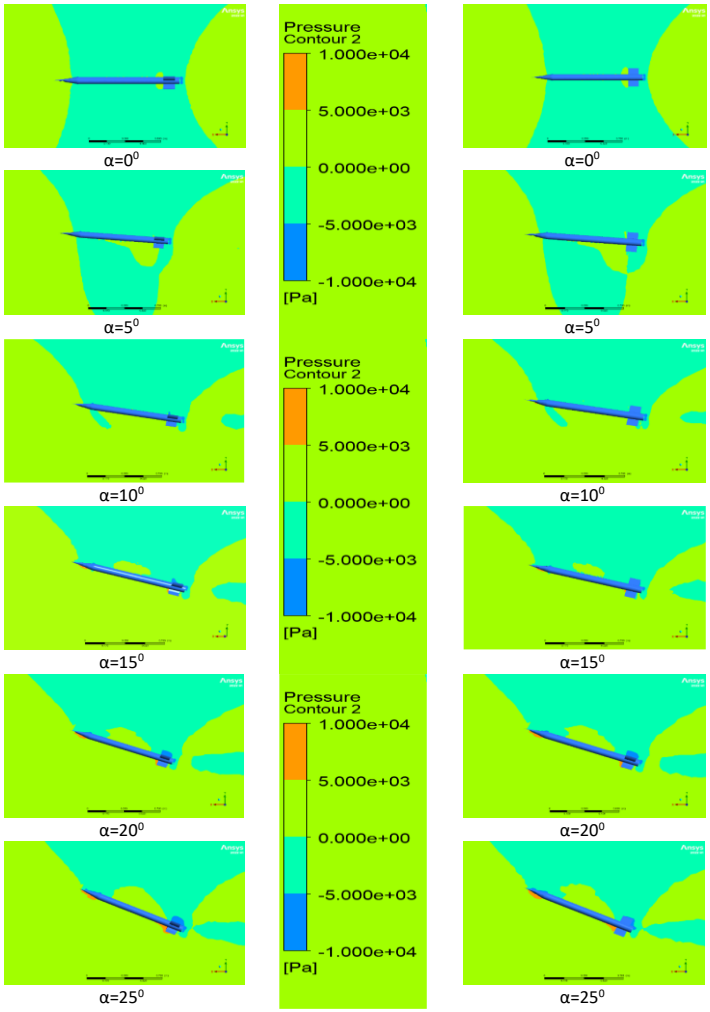

Fig. 11. (a) Mach 0.6 Curved Fin Rocket Pressure Contour, (b) Mach 0.6 Straight Fin Velocity Contour Rocket

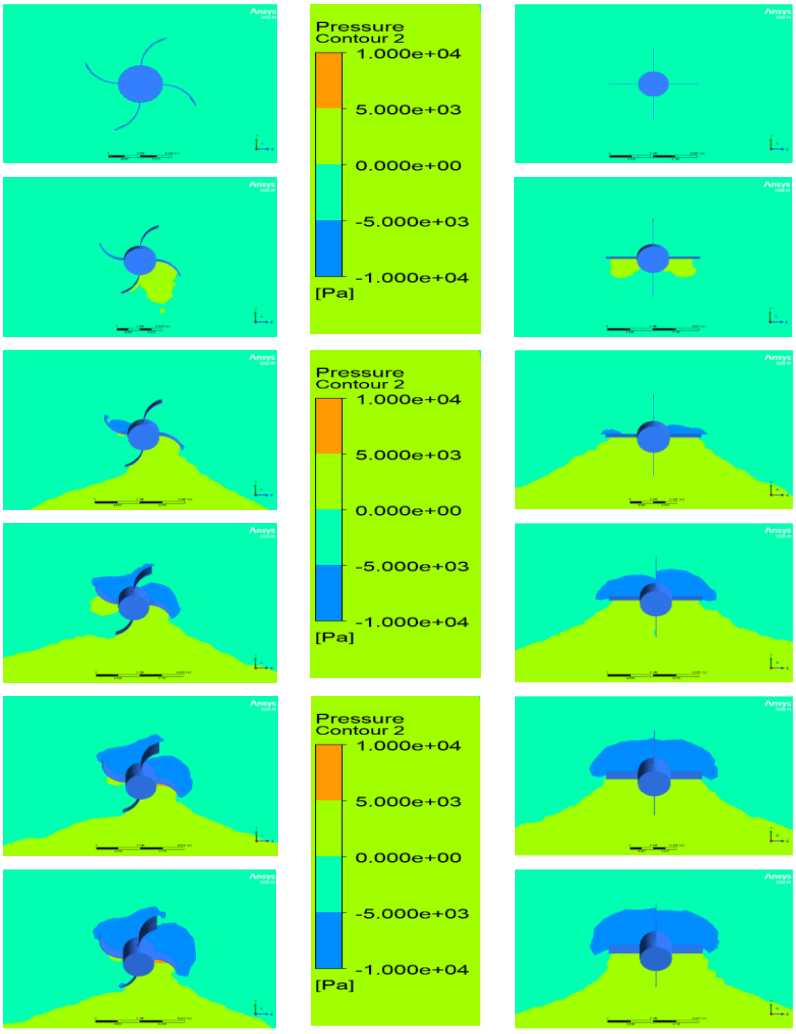

Fig. 12. Boundary Condition

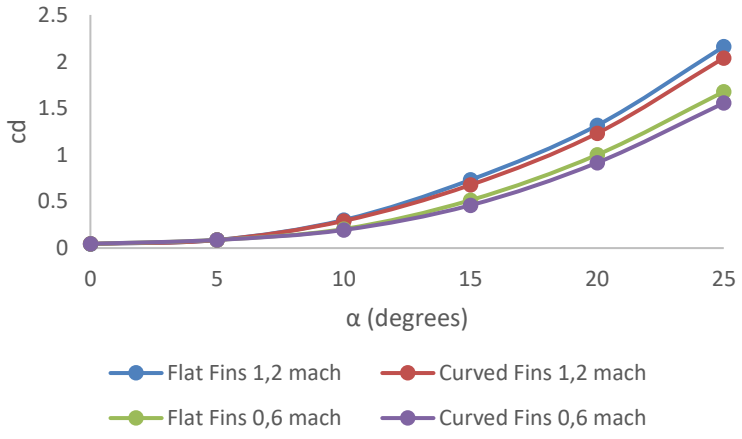

Fig. 13. Cofficient drag value

To validate the results of this research by looking at the simulation results in Dahalan's *et al.,* [3] study. Dahalan *et al.,* [3] conducted a study of the aerodynamic characteristics of curved fin rockets using semi-empirical methods and numerical simulations. In this study, the results obtained from wind tunnel testing, USAF DATCOM, and numerical simulations were compared with each other. Meanwhile, this study compares the aerodynamic properties of curved fin rockets with straight fin

rockets using CFD simulations. Figure 14 shows the comparison results between the simulations carried out by Dahalan *et al.,* [3] and this study.

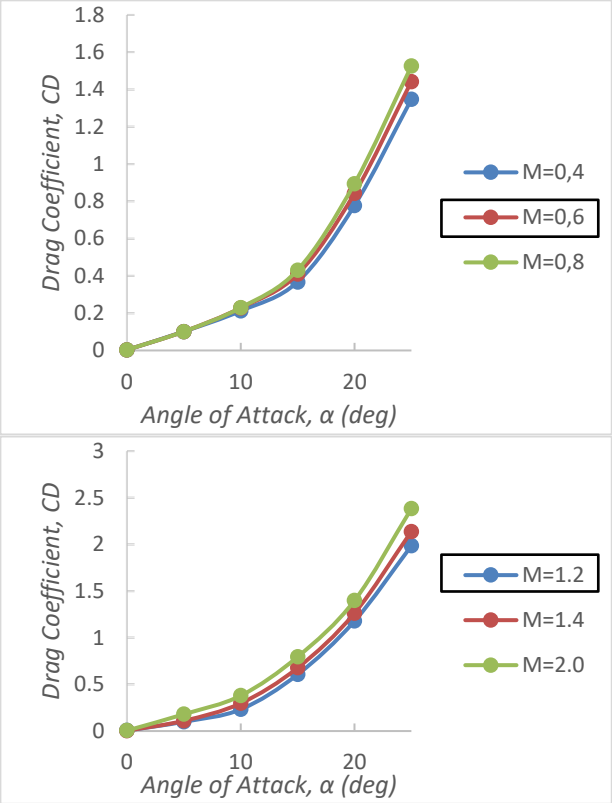

AoA (α)	Dahalan's *et al.,* [3] result	This work	Error
0^0	0,04054	0,03845192	5,15 %
5^0	0,07541	0,072133812	4,34 %
10^0	0,17702	0,1709055	3,45 %
15^0	0,42713	0,40491924	5,21 %
20^0	0,89610	0,860256	4,10 %
25^0	1,51357	1,44545935	4,52 %

AoA (α)	Dahalan's *et al.,* [3] result	This work	Error
0^0	0,05045	0,049814	5,22 %
5^0	0,09697	0,09276473	4,33 %
10^0	0,23243	0,24041566	3,43 %
15^0	0,60631	0,63975324	5,51 %
20^0	1,15885	1,2111565	4,51 %
25^0	1,99477	2,096492	5,09 %

Fig. 14. Results of previous work validation by Dahalan *et al.,* [3]

The CFD simulation results in Ansys show that the lift coefficient (cl) (Figure 15) for both straight and curved fins continue to increase with AoA ranging from 0 to 250 degrees and velocities of 0.6 and 1.2 Mach. The straight-fin rocket has a higher CL value than the curved-fin rocket due to the larger lift area or pressure difference between the upper and lower surfaces of the fin.

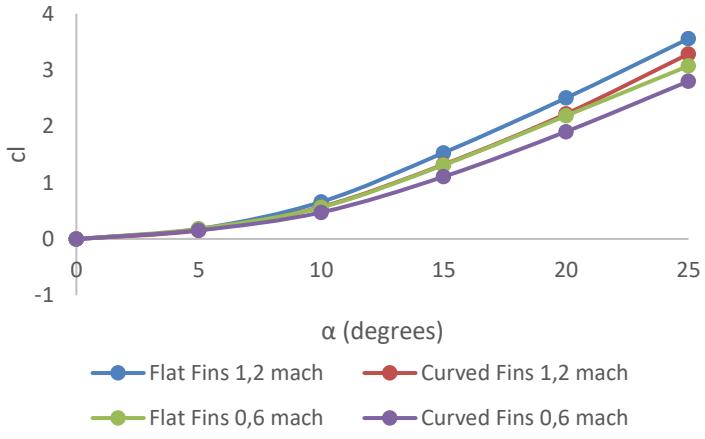

Fig. 15. Coefficient lift value

Figure 16 represents the output results of the pitching moment coefficient (cm) from the Ansys simulation, with variations in AoA ranging from 0 to 250 degrees and Mach numbers of 0.6 and 1.2. Both the flat and curved fin rockets have negative values of the pitching moment coefficient, with

increasing AoA. Among the two types of fin rockets, the highest cm value occurs for the curved-fin rocket because the flow around the curved fin can create turbulence or pressure changes that result in a rotational moment.

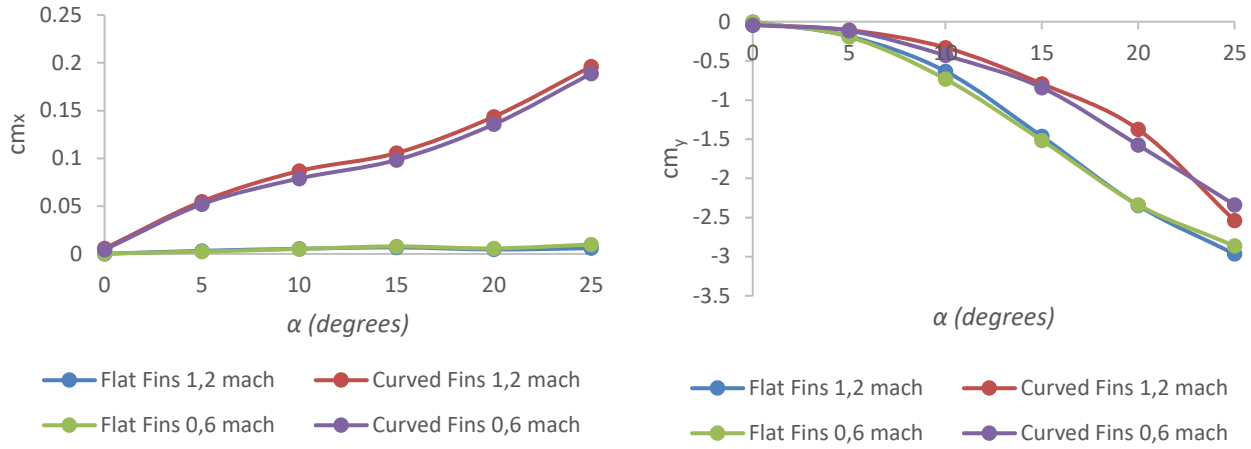

(a) (b)

Fig. 16. (a) rolling moment coefficient; (b) pitching moment coefficient

The rolling moment shown in Figure 17 shows that there is a difference between straight fin rockets and curved fin rockets. In curved fin rockets there is an increase in the rolling moment value with increasing angle of attack, whereas in flat fin rockets the rolling moment tends to be stable, namely close to 0. The comparison between the rolling moment coefficient and the pitching moment coefficient between straight fin and curved fin rockets is very different, based on the results of this simulation. However, based on the data above, it shows that curved fin rockets have higher values than flat fin rockets in terms of rolling moment and pitching moment coefficient.

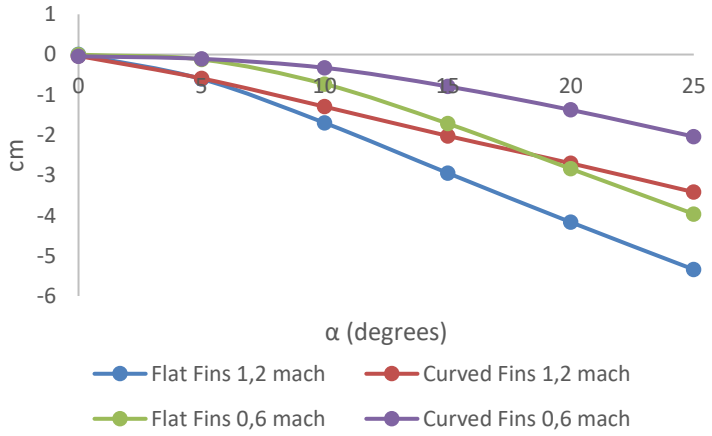

Fig. 17. Coefficient moment value

To determine which type of fin rocket performs better, a comparison of the cl/cd ratio is needed because a lower cd value and higher cl value do not necessarily indicate better aerodynamic performance. From the simulation results, it is found that the highest cl/cd value occurs for the straight-fin rocket with a velocity of 0.6 Mach. The graph in Figure 18 also shows that both rockets achieve improved performance at an AoA of 10 degrees, suggesting that both types of rockets would benefit from launching at an angle of attack of 10 degrees.

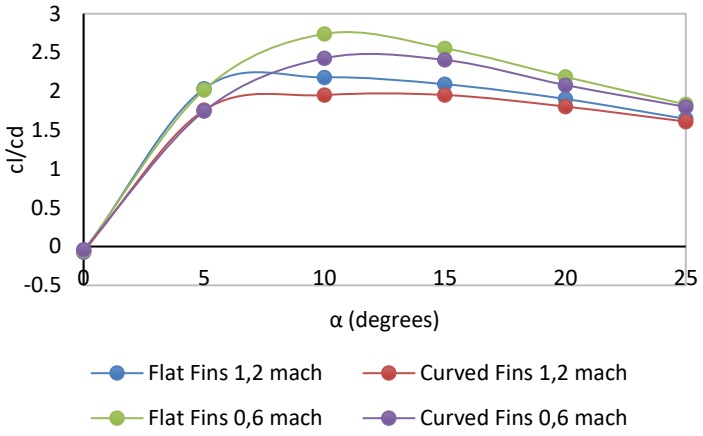

Fig. 18. The value of CL/CD

4. Conclusions

During this study, diverse fin configurations were meticulously modelled and subjected to simulation within the ANSYS environment. The analysis of simulation outcomes yields the discernment that heightened angles of attack prompt air separation and induce substantial pressure differentials along the rocket's surface. This phenomenon culminates in elevated values of both drag coefficient (*Cd*) and lift coefficient (*Cl*) for rockets featuring both curved and straight fins. Notably, the straight-fin rocket manifests the highest *Cd* and *Cl* values, attributable to its augmented surface area in contact with the airstream compared to its curved-fin counterpart. Optimal aerodynamic performance, as indicated by the zenith of the *Cd* and *Cl* ratio, is attained by both curved and straight-fin rockets at an angle of attack of 10 degrees. However, a nuanced comparison reveals that the flat-fin rocket surpasses the curved-fin variant in performance owing to its superior CL and CD ratio. This empirical substantiation underscores the imperative role of fin configuration in influencing aerodynamic parameters, elucidating the comparative advantages of specific designs under varying aerodynamic conditions. Thus, these findings contribute valuable insights into the optimization of rocket aerodynamics, underscoring the significance of fin geometry in enhancing overall performance metrics.

Acknowledgement

This research was funded by a grant from Research Collaboration of Indonesia (RKI 2023).

References

[1] Sutton, George P., and Oscar Biblarz. *Rocket propulsion elements*. John Wiley & Sons, 2016.

[2] Gomez, Faustino J., and Risto Miikkulainen. "Active guidance for a finless rocket using neuroevolution." In *Genetic and Evolutionary Computation Conference*, pp. 2084-2095. Berlin, Heidelberg: Springer Berlin Heidelberg, 2003. https://doi.org/10.1007/3-540-45110-2_105

[3] Dahalan, Md Nizam, Ahmad Fitri Suni, Iskandar Shah Ishak, Nik Ahmad Ridhwan Nik Mohd, and Shabudin Mat. "Aerodynamic study of air flow over a curved fin rocket." *Journal of Advanced Research in Fluid Mechanics and Thermal Sciences* 40, no. 1 (2017): 46-58.

[4] Zhang, G. Q., L. C. Ji, Y. Xu, and J. Schlüter. "Parametric study of different fins for a rocket at supersonic flow." *Proceedings of the Institution of Mechanical Engineers, Part C: Journal of Mechanical Engineering Science* 229, no. 18 (2015): 3392-3404. https://doi.org/10.1177/0954406215590642

[5] Zhang, Guo Qing, S. C. M. Yu, and J. Schlüter. "Aerodynamic characteristics of a wrap-around fin rocket." *Aircraft Engineering and Aerospace Technology: An International Journal* 88, no. 1 (2016): 82-96. https://doi.org/10.1108/AEAT-03-2014-0030

[6] Sethunathan, P., R. N. Sugendran, and T. Anbarasan. "Aerodynamic Configuration Design of a Missile." *International Journal of Engineering Research & Technology* 4, no. 3 (2015): 72-75. https://doi.org/10.17577/IJERTV4IS030060
[7] Eastman, D., and D. Wenndt. "Aerodynamics of maneuvering missiles with wrap-around fins." In *3rd Applied Aerodynamics Conference*, p. 4083. 1985. https://doi.org/10.2514/6.1985-4083
[8] Anderson, John. *Fundamentals of aerodynamics*. McGraw-Hill, 2016.
[9] Bahamon, Jhan, and Manuel Martinez. "Study of fluid-dynamic behavior in a convergent–divergent nozzle by shape optimization using evolutionary strategies algorithms." *Proceedings of the Institution of Mechanical Engineers, Part G: Journal of Aerospace Engineering* 237, no. 12 (2023): 09544100231163372. https://doi.org/10.1177/09544100231163372
[10] Sutton, George P., and Oscar Biblarz. *Rocket propulsion elements*. John Wiley & Sons, 2016.
[11] McCormick, Barnes W. *Aerodynamics, aeronautics, and flight mechanics*. John Wiley & Sons, 1994.
[12] Wissocq, Gauthier, Said Taileb, Song Zhao, and Pierre Boivin. "A hybrid lattice Boltzmann method for gaseous detonations." *Journal of Computational Physics* 494 (2023): 112525. https://doi.org/10.1016/j.jcp.2023.112525
[13] Park, Seong-Ho, Thanh-Hoang Phan, Van-Tu Nguyen, Trong-Nguyen Duy, Quang-Thai Nguyen, and Warn-Gyu Park. "Numerical simulation of wall shear stress and boundary layer flow from jetting cavitation bubble on unheated and heated surfaces." *International Journal of Heat and Mass Transfer* 222 (2024): 125189. https://doi.org/10.1016/j.ijheatmasstransfer.2024.125189
[14] Panagiotou, P., P. Kaparos, and K. Yakinthos. "Winglet design and optimization for a MALE UAV using CFD." *Aerospace Science and Technology* 39 (2014): 190-205. https://doi.org/10.1016/j.ast.2014.09.006
[15] Narayan, Gautham, and Bibin John. "Effect of winglets induced tip vortex structure on the performance of subsonic wings." *Aerospace Science and Technology* 58 (2016): 328-340. https://doi.org/10.1016/j.ast.2016.08.031
[16] Wells, Jesse, Abdel-Halim Salem Said, and Saad Ragab. "Effects of turbulence modeling on RANS simulations of tip vortices." In *48th AIAA Aerospace Sciences Meeting Including the New Horizons Forum and Aerospace Exposition*, p. 1104. 2010. https://doi.org/10.2514/6.2010-1104
[17] Kadivar, Mohammadreza, David Tormey, and Gerard McGranaghan. "A comparison of RANS Models used for CFD prediction of turbulent flow and heat transfer in rough and smooth channels." *International Journal of Thermofluids* (2023): 100399. https://doi.org/10.1016/j.ijft.2023.100399